Available online at www.sciencedirect.com

jmr&t Journal of Materials Research and Technology

journal homepage: www.elsevier.com/locate/jmrt

Original Article

Alterations in the magnetic and electrodynamic properties of hard-soft $Sr_{0.5}Ba_{0.5}Eu_{0.01}Fe_{12}O_{19}$/$Ni_xCu_yZn_wFe_2O_4$ nanocomposites

M.A. Almessiere [a,b,**], Y. Slimani [b,***], H. Attia [c], S.I.M. Sheikh [c], Ali Sadaqat [d], M.G. Vakhitov [e,f], D.S. Klygach [e,f], M. Sertkol [g], A. Baykal [h], A.V. Trukhanov [e,i,j,*]

[a] Department of Physics, College of Science, Imam Abdulrahman Bin Faisal University, P.O. Box 1982, Dammam, 31441, Saudi Arabia

[b] Department of Biophysics, Institute for Research and Medical Consultations (IRMC), Imam Abdulrahman Bin Faisal University, P.O. Box 1982, Dammam, 31441, Saudi Arabia

[c] Electrical Engineering Department, King Fahd University of Petroleum and Minerals, Dhahran, 31261, Saudi Arabia

[d] Mechanical and Energy Engineering Department, College of Engineering, Imam Abdulrahman Bin Faisal University, P.O. Box 1982, Dammam, 31441, Saudi Arabia

[e] South Ural State University, Chelyabinsk, 454080, Russia

[f] Ural Federal University, Ekaterinburg, 620002, Russia

[g] Deanship of Preparatory Year Building 450, Imam Abdulrahman Bin Faisal University, P.O. Box 1982, Dammam, 31441, Saudi Arabia

[h] Department of Nanomedicine Research, Institute for Research and Medical Consultations (IRMC), Imam Abdulrahman Bin Faisal University, P.O. Box 1982, Dammam, 31441, Saudi Arabia

[i] SSPA "Scientific and Practical Materials Research Centre of NAS of Belarus", Minsk, 220072, Belarus

[j] L.N. Gumilyov Eurasian National University, Nur-Sultan, 010000, Kazakhstan

ARTICLE INFO

Article history:
Received 25 June 2021
Accepted 29 August 2021
Available online 7 September 2021

Keywords:
Hard-soft nanocomposites
Spinel ferrites
Hexaferrite
Microwave absorption
Magnetic properties

ABSTRACT

Hard/soft (H/S) $Sr_{0.5}Ba_{0.5}Eu_{0.01}Fe_{12}O_{19}$/$Ni_xCu_yZn_wFe_2O_4$ nanocomposites (NCs) were produced via a *one-pot* sol–gel auto-combustion procedure. Phase and surface analyses were performed using X-ray diffraction (XRD), scanning electron microscopy (SEM), transmission electron microscopy (TEM), and high-resolution transmission electron microscopy (HR-TEM). Magnetization measurements for H/S NCs with different x, y, and w ratios were investigated at two different temperatures (300 and 10 K). The M–H curves were not smooth for the different H/S NCs, revealing that the exchange interaction was incomplete. The derivative of the magnetization (dM/dH versus H) exhibited two separate peaks, confirming the non-coupled H/S mixtures. Maximum saturation magnetization (M_s) values of 93.9 and 63.1 emu/g were obtained at 10 and 300 K, respectively, for the H/S $Sr_{0.5}Ba_{0.5}Eu_{0.01}Fe_{11.99}O_{19}$/$Ni_{0.3}Cu_{0.3}Zn_{0.4}Fe_2O_4$ NC, which contained the highest content of Zn and the

* Corresponding author.
** Corresponding author.
*** Corresponding author.
E-mail addresses: malmessiere@iau.edu.sa (M.A. Almessiere), yaslimani@iau.edu.sa (Y. Slimani), truhanov86@mail.ru (A.V. Trukhanov).

https://doi.org/10.1016/j.jmrt.2021.08.137

same contents of Ni and Cu within the soft magnetic phase. The calculated squareness ratios (SQR = M_r/M_s) were less than 0.5, indicating incomplete exchange coupling. The coercive field (H_c) of the produced NCs reached a maximum value of approximately 2485 Oe at 300 K and 2331 Oe at 10 K with a decrease in the M_s values to 56.9 emu/g at 300 K and 78.5 emu/g at 10 K for the H/S $Sr_{0.5}Ba_{0.5}Eu_{0.01}Fe_{11.99}O_{19}/Ni_{0.8}Cu_{0.1}Zn_{0.1}Fe_2O_4$ NC, which contained lower fractions of Zn and Cu and the highest fraction of Ni. The reflection/transmission-based waveguide approach was employed to investigate the electrodynamic properties of the H/S NC samples within a frequency band of 7–18 GHz. The reflection and transmission coefficients (S_{11}/S_{21}) were measured using a vector network analyzer (VNA) for the sample placed inside a waveguide. The frequency dispersions of the magnetic permeability and electric permittivity were calculated.

1. Introduction

Spinel ferrites play important roles owing to their ease of synthesis, chemical stability, and high electrical resistivity. They are employed in numerous areas, such as data storage, sensors, medicines, telecommunications, photo-catalysts, microwave, magneto-optical, cancer treatment, and photo-active materials [1–4]. In recent years, hard/soft (H/S) nanocomposites (NCs) have been utilized extensively owing to their exceptional microwave absorption, electromagnetic (EM), and magnetization characteristics [5,6]. There are numerous composites based on hard/soft ferrites, such as $Ni_{0.5}Zn_{0.5}Fe_2O_4/BaFe_{12}O_{19}$ [7], $NiFe_2O_4/SrCo_{0.2}Fe_{11.8}O_{19}$ [8], $Ni_{0.6}Zn_{0.4}Fe_2O_4/SrFe_{12}O_{19}$ [9], $SrFe_{12}O_{19}/FeCo$ [10], $BaFe_{12}O_{19}/CoFe_2O_4$ [11], $Mn_{0.6}Zn_{0.4}Fe_2O_4/Sr_{0.85}Ba_{0.15}Fe_{12}O_{19}$ [12], $Ni_{0.5}Zn_{0.5}Fe_2O_4/SrFe_{12}O_{19}$ [13], $SrFe_{12}O_{19}/Ni_{0.5}Zn_{0.5}Fe_2O_4$ [14], $BaFe_{12}O_{19}/CoFe_2O_4$ [15], $Li_{0.3}Co_{0.5}Zn_{0.2}Fe_2O_4/SrFe_{12}O_{19}$ [16], and $(Mn_{0.8}Mg_{0.2}Fe_2O_4)_{(1-x)}/(BaZn_{0.15}Al_{0.15}Fe_{11.7}O_{19})_x$ [17]. It has been determined that a high coercive field (H_c) and high saturation magnetization (M_s) can be realized via exchange coupling of the hard and soft phases [18,19]. Many studies have reported the behavior of exchange coupling in nanopowders, metal alloys, and thin films such as Sm–Co/Fe [20], $SmCo_x$–Co [21], $Pr_2Fe_{12}B$ [22], and FeNi/FePt [23]. Recently, nanocomposite magnetic materials have attracted attention as a result of their exceptional magnetic properties. Some significant factors have been identified, such as the grain size, magnetic interaction, composition, and microstructure of soft and hard ferrites [18]. It has been noted that the appropriate calcination process and mass ratio can improve the magnetic properties of H/S ferrites [24,25]. It is difficult to realize high magnetic saturation and high coercivity simultaneously because most magnetic materials exhibit a high value of coercivity and a low magnetization saturation [26]. Consequently, it is necessary to synthesize composite materials to achieve the exchange coupling of hard and soft magnetic structures [27,28]. In addition, spinel hard and soft ferrite composites have excellent electrical resistivity and high corrosion resistance [14]. Soft spinel ferrites play an important role in microwave applications because of their less anisotropic properties [29]. It has been reported that hard hexagonal ferrites (such as $BaFe_{12}O_{19}$) exhibit excellent anisotropy and a high resonant frequency that is adequate up to the W-band [30]. Consequently, the chemistry of highly anisotropic hard ferrites and slightly anisotropic soft ferrites can be used for diverse microwave applications [31,32], such as the construction of radar-absorbing materials (RAM) used for military and defense applications [5]. Nevertheless, a wideband frequency range, thin absorption layer, and high absorption peak cannot be achieved with a single material of an exemplary radar [6,33]. The exchange between hard and soft ferrite phases constructs standard nanocomposites that may be useful and appropriate [34]. The magnetic and dielectric nanocomposites exhibit high permeability (μ_r) and large permittivity (ε_r) attributable to the exchange-coupling effect. However, certain nanocomposites operating at frequencies in the range of 12–18 GHz are used in military and sensitive applications [35,36]. Functional composites based on transition metal oxides (Fe_3O_4, $BaFe_{12-x}D_xO_{19}$) with a polymer matrix [37,38] have been widely investigated.

With the synthesis and development of new nanocomposite materials and their varied use in new applications, it has become crucial to employ highly accurate techniques for the characterization of their EM properties [39–41]. Furthermore, this characterization must be viable for a broad spectrum of materials. Nondestructive testing (NDT), which serves as a tool to characterize nanocomposite materials without causing any damage to the sample or permanently altering its structure, can be adopted through EM techniques to measure material properties smoothly and accurately. Typical reflection/transmission (R/T) or reflection-only NDT methods include free-space reflection and open-ended probe techniques [39–44]. These are preferred as they do not disrupt the material integrity, and they are utilized in several areas such as the biomedical, construction, and mechanics fields. However, these methods are inaccurate and complex in mathematical modeling compared with guided R/T techniques based on microwave waveguides.

As such, it is important to characterize the EM properties of H/S NCs accurately to remove sources of error in this study. Various characterization techniques have been reported in the scientific literature [44–46]. These can be broadly categorized into two groups: *resonance techniques and R/T methods*. Resonance techniques can deliver highly accurate EM characterization, although the sample under study and the designed resonator need to be fabricated with a great degree of precision [45]. Additionally, these methods are generally limited to a narrow range of materials and the measurement of properties

such as permeability, permittivity, and the sample size. The challenges associated with resonance techniques include their cost and impracticality when used in research laboratories where material characterization is not the primary focus, but rather serves as the first step in the design of a device.

On the other hand, R/T methods based on EM devices such as coaxial lines, waveguides, and free-space propagation can be used to characterize composite materials. R/T characterization is a wideband method, unlike other methods that work on single or multiple frequencies. The working frequency band for performing the characterization is dependent on the type of R/T device used for measurement. Waveguides and coaxial cables employ a unimodal propagation band for material characterization. Coaxial cables are practical as they can provide a wider bandwidth and, in theory, support low-frequency measurements owing to the absence of a cut-off band. The problem with this technique is that the material should be prepared in such a shape that it can conform to the concentric corona of the cable, which is problematic from a manufacturing perspective. On the other hand, waveguide characterization requires simpler sample preparation, which makes it preferable to the use of coaxial cables, despite its lower allowable bandwidth.

The R/T-based waveguide approach is used to study the electrodynamic properties of H/S S1–S5 NCs in this study. First, the coefficients of the reflected and transmitted energy (S_{11}–S_{21}) are measured using a vector network analyzer (VNA) for a sample placed in a waveguide with a cut-off frequency of 7 GHz. Consequently, the frequency dispersions of the permittivity and magnetic permeability are calculated based on the measured S_{11}–S_{21}.

Therefore, we have selected a nano-composition consisting of $Sr_{0.5}Ba_{0.5}Eu_{0.01}Fe_{12}O_{19}$ as a hard ferrite and $Ni_xCu_yZn_wFe_2O_4$ as a soft ferrite. These materials were selected based on the improvement in the structural and magnetic properties of Eu-doped M-type hexaferrite and Ni–Zn–Cu spinel ferrite according to various research reports. C. Liu et al. studied the impact of Eu substitution in Sr-hexaferrites on their structure and magnetic features [46]. They found that there was a considerable improvement in the saturation magnetization (M_s) and intrinsic coercivity (H_c) with substitution Moreover, A. Zafar et al. investigated the electrical and magnetic characteristics of Eu-doped barium hexaferrites. The samples exhibited a decreased conductivity and increased saturation magnetization and coercivity with Eu doping [47]. B. Thangjam et al. and D. Venkatesh et al. explored the magnetic properties of Cu-substituted Ni–Zn spinel ferrites. They observed superior magnetic characteristics when the Cu concentration was varied [48,49]. As a result, we produced H/S $Sr_{0.5}Ba_{0.5}Eu_{0.01}Fe_{12}O_{19}$/$Ni_xCu_yZn_wFe_2O_4$ (S1–S5) NCs and explored the effects of varying the Ni, Cu, and Zn ratios on the structural parameters and magnetic and microwave (MW) properties. To the best of our knowledge, there have been no similar studies on this composition, and thus the results presented here can contribute significantly to the research field of H/S ferrite NCs.

2. Experimental

For the H/S $Sr_{0.5}Ba_{0.5}Eu_{0.01}Fe_{12}O_{19}$/$Ni_xCu_yZn_wFe_2O_4$ NCs, x = 0.2, y = 0.4, w = 0.4 is denoted as sample S1; x = 0.3, y = 0.3, w = 0.4 is sample S2; x = 0.4, y = 0.4, w = 0.2 is sample S3; x = 0.6, y = 0.2, w = 0.2 is sample S4; and x = 0.8, y = 0.1, w = 0.1 is sample S5. The H/S NC samples were produced via a *one-pot* sol–gel citric auto-combustion approach. To prepare the $Sr_{0.5}Ba_{0.5}Eu_{0.01}Fe_{12}O_{19}$ solution, specific amounts of $Sr(NO_3)_2$, $Ba(NO_3)_2$, $Eu(NO_3)_3$, and $Fe(NO_3)_3 \cdot 9H_2O$ were mixed with 80 mL of DI H_2O and stirred at 80 °C for 15 min. The $Ni_xCu_yZn_wFe_2O_4$ solutions were synthesized by mixing certain ratios of $Ni(NO_3)_2$, $Zn(NO_3)_2$, $Cu(NO_3)_2$, and $Fe(NO_3)_3 \cdot 9H_2O$ according to the chemical formulas for samples S1–S5 with 80 mL of DI H_2O and stirring at 80 °C for 15 min. Subsequently, the solutions of $Sr_{0.5}Ba_{0.5}Eu_{0.01}Fe_{12}O_{19}$ and each $Ni_xCu_yZn_wFe_2O_4$ composition were mixed, and $C_6H_8O_7$ was added with continuous stirring for 30 min. Subsequently, the pH of the solutions was adjusted by adding ammonium solution to reach pH 7, and the solutions were held at 165 °C for 1 h and then heated to 350 °C until the solution turned into a viscous gel. Then, the gel was heated until it burned completely to obtain a fluffy black powder that was sintered at 950 °C for 6 h.

The formation of the products was confirmed using x-ray diffraction (XRD) with a Rigaku D/MAX-2400. Surface and microstructural analyses were performed using a Tescan field emission scanning electron microscope (FE-SEM) with energy dispersive x-ray spectroscopy (EDX) and a Titan

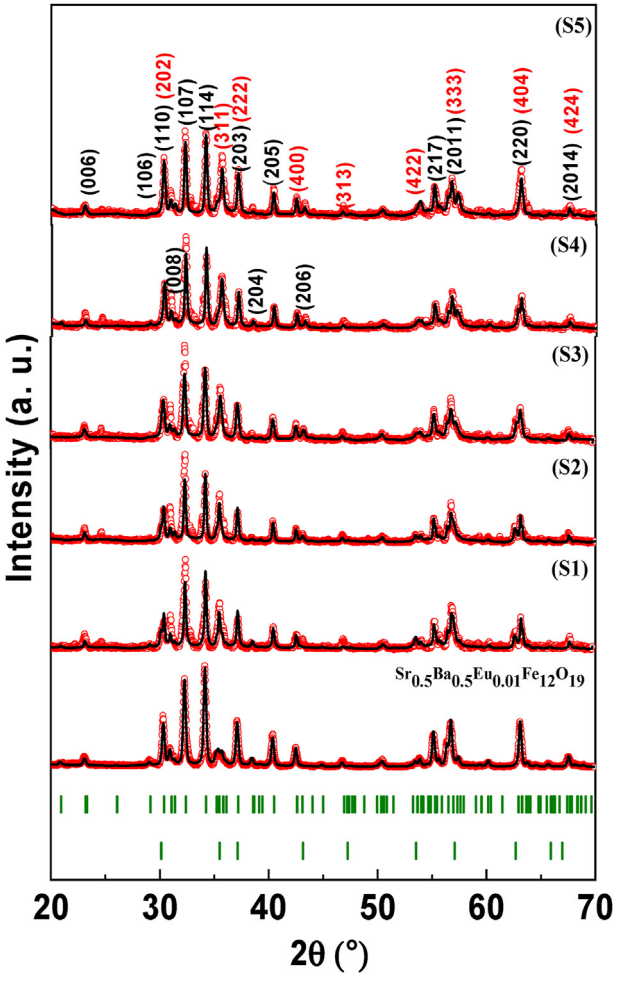

Fig. 1 – Powder XRD patterns of S1–S5 H/S NCs.

Table 1 – Determined structural parameters for various H/S NCs.

Product	D_{XRD} (nm)		Hard phase			Soft phase	
	Soft	Hard	a = b (Å)	c (Å)	Fraction (%)	a = b = c (Å)	Fraction (%)
$Sr_{0.5}Ba_{0.5}Eu_{0.01}Fe_{12}O_{19}$	–	67.1	5.8934	23.1314	100	–	–
S1	48.6	84.6	5.8823	23.0820	78.7	8.4388	21.3
S2	48.2	78.6	5.8843	23.0958	79.5	8.4024	20.5
S3	39.9	62.5	5.8872	23.0961	78.5	8.3665	21.5
S4	33.9	54.5	5.8864	23.0980	73.0	8.3502	27.0
S5	20.0	52.3	5.8830	23.0851	72.9	8.3611	27.1

transmission electron microscope (TEM). The magnetic properties of the products were investigated using a Quantum Design SQUID-PPMS vibrating sample magnetometer (PPMS DynaCool, Quantum Design, San Diego, CA, USA). The MW properties in the range of 7–18 GHz were calculated for the five investigated samples using an Agilent VNA (Model E5071C) employing the transmission-line approach for the measurement. The samples were placed inside a rectangular waveguide to interfere with the propagating waves. The measured coefficients of the reflected (S_{11}) and transmitted (S_{21}) energies were transformed to permittivity and permeability values (real and imaginary parts) using the Nicolson–Ross–Weir algorithm [38] based on the measured S-parameters at different frequencies.

3. Results and discussion

3.1. Microstructure

The XRD patterns of the S1–S5 H/S NCs are illustrated in Fig. 1. The XRD patterns of several NCs presented peaks associated with spinel ferrite and Sr–Ba hexaferrite, which confirms the occurrence of hard and soft phases together with no configuration of any secondary phases. The cell parameters of the S1–S5 H/S NCs and the proportions of both hard and soft ferrites were estimated using Match! v. 3 Full Proof software and are listed in Table 1. The cell parameters of both phases fluctuated slightly with changes in the ratios of Ni, Cu, and Zn in the soft side because of the redistribution of ions in the spinel structure [46]. Furthermore, the crystallite size (D_{XRD}) of the S1–S5 H/S NCs was obtained using the Scherrer equation. The crystallite size decreased with the variation in the amounts of Ni, Cu, and Zn. Moreover, the crystal size of the hard phase was nearly 57% greater than that of the soft phase [47]. The variation in crystallite size is due to the boundary migration that generally occurs through extended-range diffusion among hard and soft phase systems [48].

3.2. Morphological investigation

The FE-SEM analysis of $Sr_{0.5}Ba_{0.5}Eu_{0.01}Fe_{12}O_{19}$ and the S1–S5 H/S NCs is shown in Fig. 2. The images show an

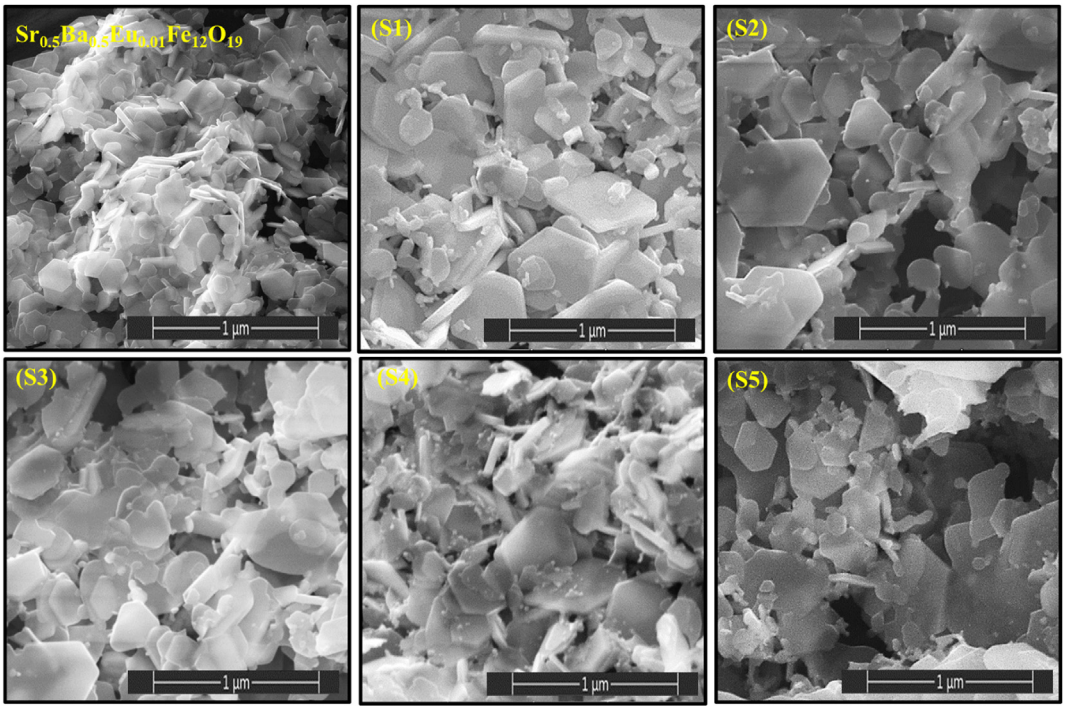

Fig. 2 – SEM micrographs of the S1–S5 H/S NCs.

accumulation of hexagonal grains, which belong to the hard ferrite, with small spherical grains of soft ferrite distributed uniformly on the top surface of the hexagonal grains; this confirms the co-occurrence of both soft and hard phases. Additionally, these observations were confirmed by the TEM images of the S2 and S4 H/S $Sr_{0.5}Ba_{0.5}Eu_{0.01}Fe_{12}O_{19}/Ni_xCu_y$-$Zn_wFe_2O_4$ NCs, as shown in Fig. 4. The images confirm the assembly of hexagonal grains covered by small spherical grains. Moreover, the co-formation of H/S NCs was confirmed via HR-TEM by measuring the lattice space for hard and soft NCs, as shown in Fig. 4. Elemental analysis of the S2 and S3 H/S $Sr_{0.5}Ba_{0.5}Eu_{0.01}Fe_{12}O_{19}/Ni_xCu_yZn_wFe_2O_4$ NCs was performed via EDX and elemental mapping (Fig. 3). The results demonstrate the presence of Sr, Ba, Eu, Ni, Zn, Cu, Fe, and O, which confirms the creation of the H/S phase without any impurities.

3.3. *Magnetization*

Before investigating the magnetic features of the S1–S5 H/S NCs, the magnetic traits of Eu-substituted SrBa hexaferrite and NiCuZn ferrite should be discussed. According to the literature, NiCuZn spinel ferrite nanoparticles are generally soft magnetic materials displaying hysteresis loops with very high M_s and very low H_c values [49–57]. For instance, Ch. Sujatha et al. [54] examined the magnetic features of NiCuZn nano-ferrites fabricated via a sol–gel process. The materials prepared at different temperatures showed super-paramagnetic (SPM) behavior with M_s values of approximately 66.9–76.7 emu/g and very low H_c values of approximately 12–49 Oe. Additionally, the magnetic traits of NiCuZn ferrite nanoparticles produced via sol–gel combustion were analyzed by L. Yu et al. [56]. The prepared products exhibited

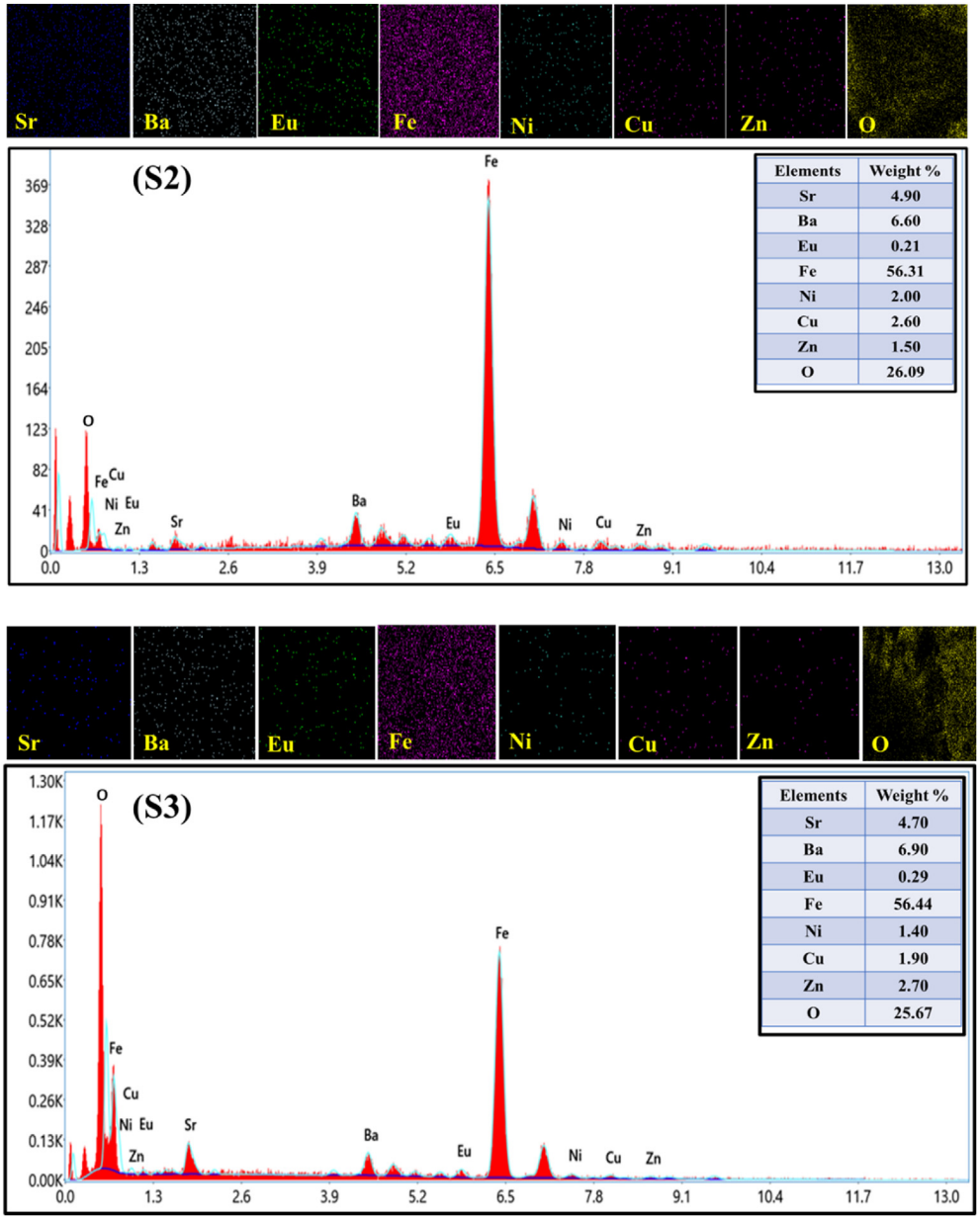

Fig. 3 – Elemental mapping and EDX spectra of the S2 and S3 H/S NCs.

soft magnetic properties with high M_s in the range of 53–72 emu/g and low H_c of 52–98 Oe. In addition, S.E. Jacobo et al. [58] examined the features of NiCuZn ferrite nanoparticles produced through the sol–gel auto-combustion process followed by calcination at various temperatures. The obtained magnetic parameters, such as M_s and H_c in the ranges of 65–84 emu/g and 11–27 Oe, respectively, revealed the soft magnetic features of the prepared nanoparticles. In another report, A.D. Karisma et al. [60] prepared nanoparticles of NiCuZn spinel ferrites through MW direct denitration. The obtained products were classified as soft magnetic nanomaterials with an M_s of 51.7 emu/g and H_c of 1.6 Oe. Similarly, Y. Slimani et al. investigated the features of NiCuZn ferrite nanoparticles substituted with different elements, such as Eu [57], Tb [59], Tm [60], and Nd–Y [61]. The non-substituted NPs exhibited SPM behavior at room temperature with M_s values that reaching 59 emu/g and H_c values of approximately 1–12 Oe, revealing their soft magnetic character. An analysis of the magnetization curves performed at 10 K illustrated a soft ferromagnetic character with a coercivity of approximately 169 Oe.

On the other hand, SrBa hexaferrites are considered hard magnetic materials, showing broad hysteresis loops with moderate M_s and high H_c values [60–64]. C. Liu et al. [46] studied the impact of Eu^{3+} ion substitution ($x = 0.00–0.25$) on the physical properties of Sr hexaferrite. A considerable enhancement of the M_s and H_c values was observed at both ambient and very low temperatures under the influence of Eu substitution. The M_s values increased continuously with increasing Eu content up to 0.15–0.20, and then decreased significantly with a further increase in Eu content. The highest H_c values of 2850 Oe at 300 K and 1338 Oe at 5 K were found in a sample with an Eu content of approximately $x = 0.10$. In another study, A. Zafar et al. [47] reported the impact of Eu doping on various physical features of Ba hexaferrite. The magnetization results indicated that M_s improved from approximately 30.5 to 54.3 emu/g and H_c increased from approximately 3030 to 8730 Oe with an increase in the Eu^{3+} content. The enhancements in M_s and H_c with Eu substitution have been attributed to the improvement in super-exchange interactions in the Fe^{2+}-O-Fe^{3+} molecules and the magneto-crystalline anisotropy of the product under the effect of Eu doping, respectively. Similarly, F. Khademi et al. [65] investigated the magnetic characteristics of Eu-doped Ba hexaferrites. They reported an increased coercivity of up to 6120 Oe with Eu^{3+} substitution, which is principally caused by the increase in magneto-crystalline anisotropy. I. Ali et al. [66] studied the properties of Eu-doped SrCa hexaferrite as

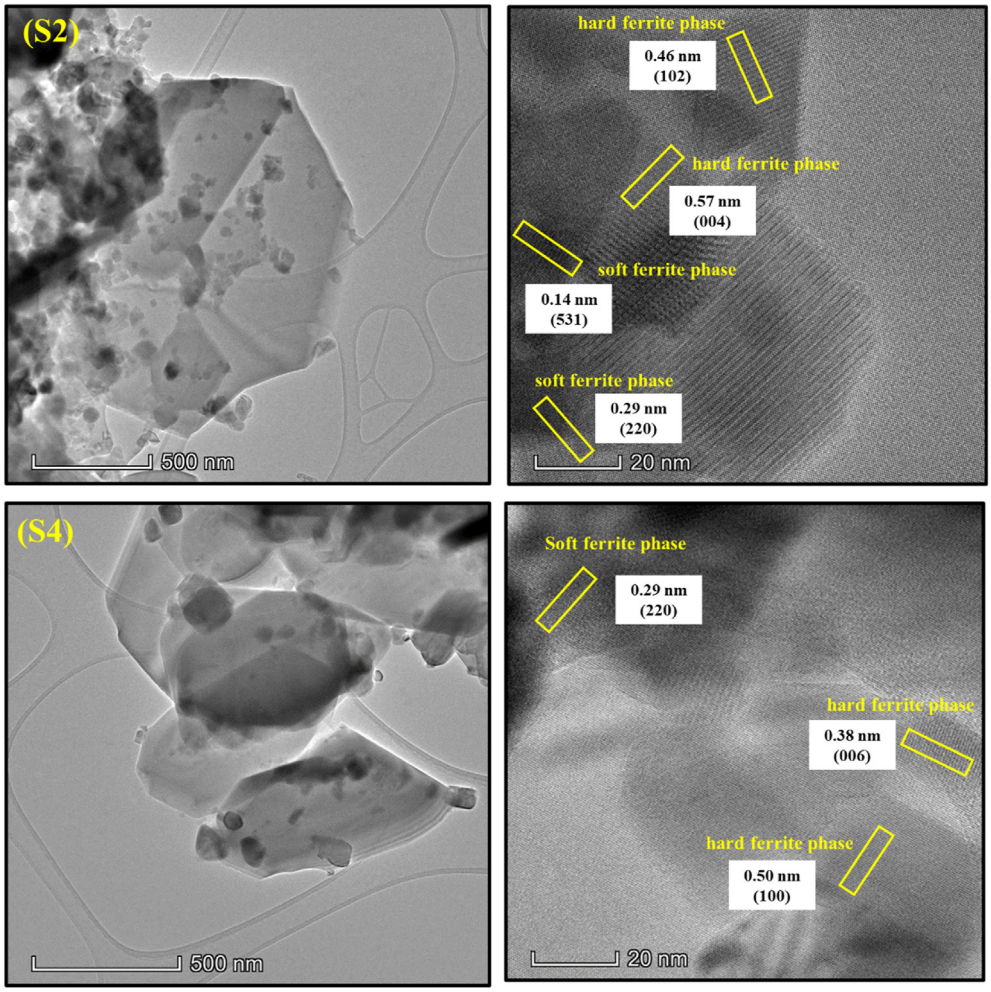

Fig. 4 – TEM and HR-TEM images of the S2 and S4 H/S NCs.

$Sr_{0.8}Ca_{0.2}Fe_{12-x}Eu_xO_{19}$ (x = 0.00–0.25). It was shown that the H_c value increased with increasing Eu^{3+} ion content, from approximately 2412 Oe for the non-substituted sample (x = 0.00) to 4045 Oe for x = 0.25. The authors attributed this enhancement to the improvement in shape anisotropy resulting from the decrease in grain size with the increase in Eu^{3+} content; thus, the inclusion of Eu plays the role of an inhibitor for the growth of grains. In a recent study, we investigated the physical properties of Eu–Nd co-substituted SrBa hexaferrite [62]. An improvement in the H_c values was observed at both 300 and 10 K under the substitution effect. The maximum H_c values were approximately 2.78 and 2.41 kOe at 300 and 10 K, respectively.

Fig. 5 illustrates the M–H data obtained at low and room temperatures for the magnetic S1–S5 H/S NCs. Magnetization measurements were conducted under an applied magnetic field of 70 kOe at both 300 and 10 K. The M–H curves are smooth for the various prepared S1–S5 H/S NCs. It has been established that a hysteresis loop with a smooth shape suggests a 'collaborative' magnetic switching of the two interacting magnetic grains across a good exchange coupling between the two phases. For the various produced NCs, the reversal in magnetization is not smooth, and the M–H curves do not exhibit a single-phase character in the second quadrant, signifying that the exchange interaction is incomplete. Based on previous reports, the exchange interaction may be significant for the magnetic characteristics of the NC when the size of the soft magnetic phase does not exceed twice the domain wall width of the hard phase [67–70]. Taking into account that the M-type hexaferrite has a domain wall width of approximately 10 nm [71], the soft magnetic phase may exhibit a mean size of approximately 20 nm.

Furthermore, Y. Sun et al. [72] confirmed these calculations and reported that the average dimension of hard magnetic grains may be greater than 40 nm. In comparison, soft magnetic grains may be smaller than approximately 20 nm to establish an excellent exchange-coupling effect. Nevertheless, here, the size of the grains for NiCuZn ferrite nanoparticles exceeds 30 nm (Table 1), which is inconsistent with the assumptions of the theoretical calculations. Hence, it will be challenging for the exchange interaction to occur between the two magnetic grains in these NCs, and consequently, the dipolar interactions will be dominant [27,73]. This results in the observation of a kink in the second quadrant of the M–H curve (Fig. 5) for NCs exhibiting weak exchange coupling.

The values of M_s, H_c, and remanence (M_r) are presented in Fig. 6 for different NCs. Maximum M_s values of 63.1 and 93.9 emu/g were obtained at 300 and 10 K, respectively, for sample S2, which contained the highest Zn content and the same Ni and Cu contents in the soft magnetic phase part. For the various produced NCs, M_r was practically the same. Generally, M_s is a fundamental characteristic of a product. Hence, it is strongly affected by the different synthesis methods, morphologies, shapes, dimensions, and structural properties of the ferrite (nano)-particles, as well as the distribution of constituent phases within the NCs [74–76]. The calculated values of the squareness ratio (SQR = M_r/M_s) are shown in Fig. 7. An SQR value of greater than 0.5 is considered a convincing criterion for the existence of the exchange coupling effect, while an SQR value of less than 0.5 is an indication on incomplete exchange between the two magnetic phases [77]. In the

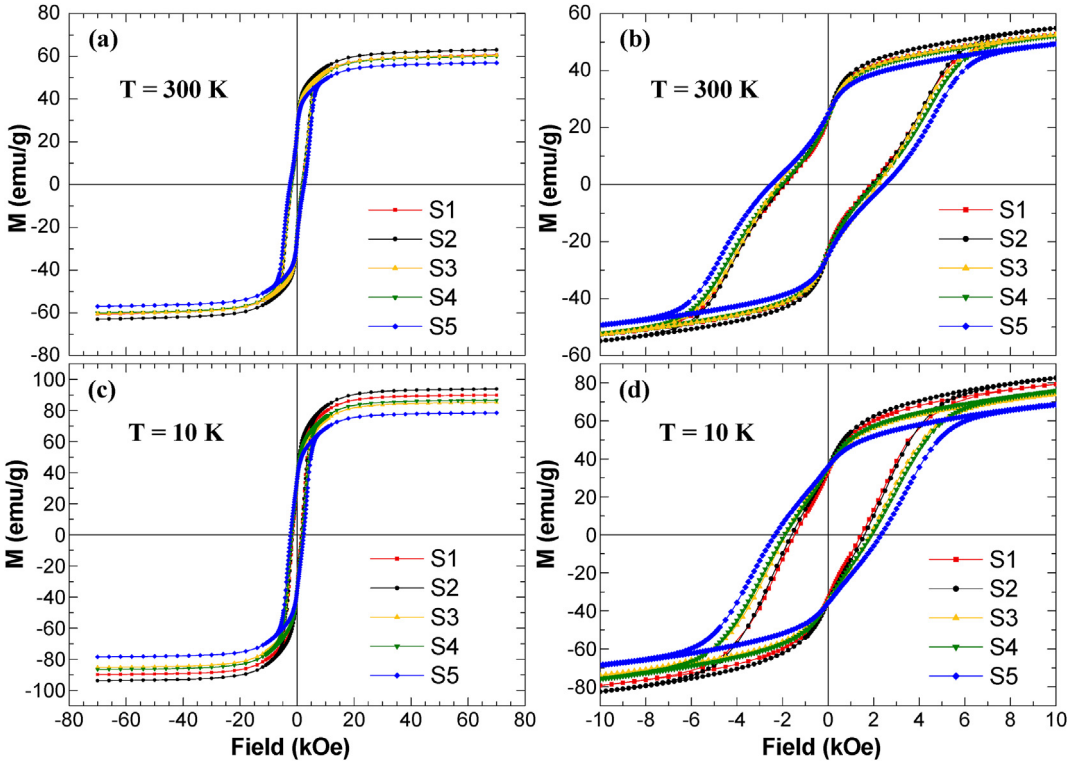

Fig. 5 – Magnetization versus field curves for S1–S5 H/S NCs performed at (a,b) T = 300 K and (c,d) T = 10 K.

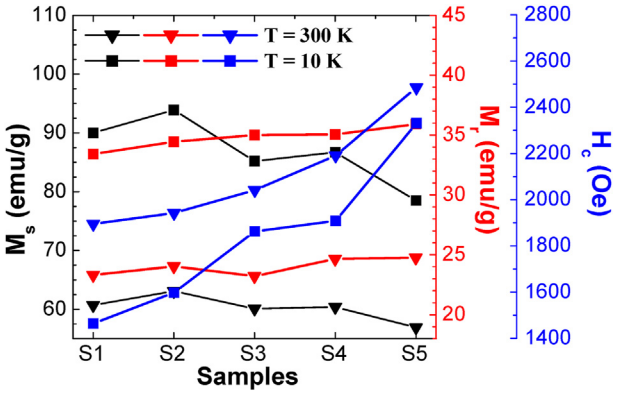

Fig. 6 – Evolution of the M_s, M_r, and H_c values for S1–S5 H/S NCs.

present study, the obtained SQR values were less than 0.5 for all of the synthesized NCs, confirming that the exchange coupling was incomplete.

The H_c values for different NCs were located amid those of the individual hard and soft magnetic phases. The coercive field of the produced NCs reached a maximum value of approximately 2485 Oe at 300 K and 2331 Oe at 10 K with a drop in M_s values to 56.9 emu/g at 300 K and 78.5 emu/g at 10 K for sample S5. This sample contained lower fractions of Zn and Cu, and the highest fraction of Ni. Without the presence of a soft phase, the magnetic moments of the hard grains are coupled, leading to deviations in the magnetic moments from the easy axis. Generally, when the soft phase is inserted into the hard grains, the effect of dipolar interactions is weakened owing to the appearance of hard–soft interactions in addition to the direct hard–hard coupling interaction. For the lower soft phase fraction, the hard grains exert a powerful exchange force on the magnetic moments of the soft grains, and hence the coercivity will be increased. However, above a certain level, when the soft fraction increases, the exchange coupling will be reduced, while the dipolar interactions (soft–soft interactions) will become significant [27,73]. Thus, the coercive field will decrease. Furthermore, some soft grains may switch the magnetic moments of the neighboring hard grains once the demagnetizing field is reversed. The extra demagnetizing field can also reduce the coercive field in the whole NC [67]. Additionally, numerous factors, including the interface condition, morphology, and grain size, affect the coercivity. Quantification of these diverse parameters is challenging. Therefore, it is difficult to monitor the coercive force in NCs.

The magnetization curves were differentiated to assess the tendency of irreversible susceptibility with respect to the reversing field. Fig. 8 presents the plots of dM/dH versus H at 300 and 10 K for different NCs. Such an analysis can provide information about the interphase exchange coupling. Typically, two separate peaks are anticipated for non-coupled H/S mixtures, whereas a single peak is observed for well-exchanged composites [78,79]. Additionally, the width of the dM/dH peaks is an indicator of the effectiveness of the H/S interphase exchange coupling. The wider the peaks, the worse the exchange coupling between the hard and soft phases is. The manifestation of a maximum in the vicinity of zero fields suggests that a large fraction of soft crystallites are uncoupled by the exchange effect. This broad peak shows a large range of crystallite sizes that exhibit various degrees of exchange coupling. Overall, the different NCs presented two peaks at the two measured temperatures. This indicates that the

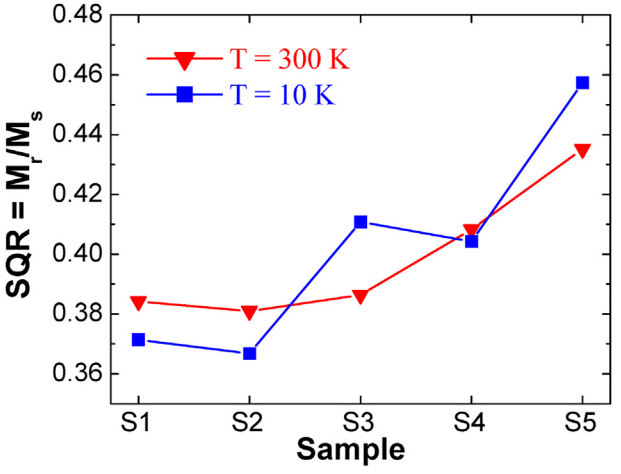

Fig. 7 – Calculated SQR values for S1–S5 H/S NCs.

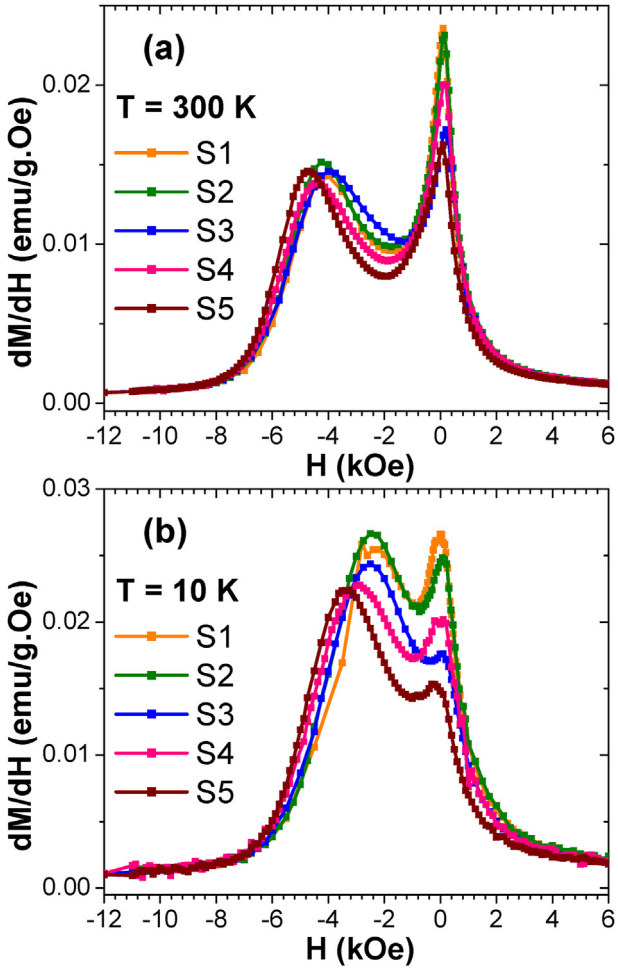

Fig. 8 – Plots of dM/dH *vs.* H for S1–S5 H/S NCs carried out at (a) T = 300 K and (b) T = 10 K.

reversal in magnetization is not accomplished in one step in these NCs.

3.4. *Microwave properties*

The MW properties of the nanocomposite samples were investigated at frequencies of 7–18 GHz using a VNA with the waveguide R/T method, as shown in Fig. 9. The permittivity (ε) and permeability (μ) values of the samples were determined using the Nicolson–Ross–Weir method based on the scattering S-parameters measured over the wide frequency range of interest [80–82]. To determine the electromagnetic parameters of the investigated materials, we used a section of the transmission line with a waveguide (air filling), as shown in Fig. 9.

Figs. 10–13 depict the dependences of the real and imaginary parts of ε and μ as functions of the frequency of the investigated composites. Because the electrodynamic parameters were measured at frequencies of 7–18 GHz, the main contributor to the formation of the dielectric constant value is the polarization losses (dipole polarization). The dipole polarization that determines the value of the real part of the permittivity is a result of the dipole orientations in the AC electric field. Because the studied material samples are a mixture of several components, the main contributors to the dielectric constant value are nickel, copper, and zinc.

The absorption of the electromagnetic field energy is manifested at frequencies coinciding with the natural frequencies of the precession of the magnetic moments of the electronic system of the ferromagnetic sample in the internal effective magnetic field. This is the excitation in the entire volume of the sample of oscillations of the uniform precession of the magnetization vector, which is caused by a magnetic microwave field. In general, this is ferromagnetic resonance. The main characteristics of ferromagnetic resonance, i.e., the resonance frequencies, relaxation, shape and width of the absorption lines, and nonlinear effects, are determined by the collective multielectron nature of ferromagnetism. In this

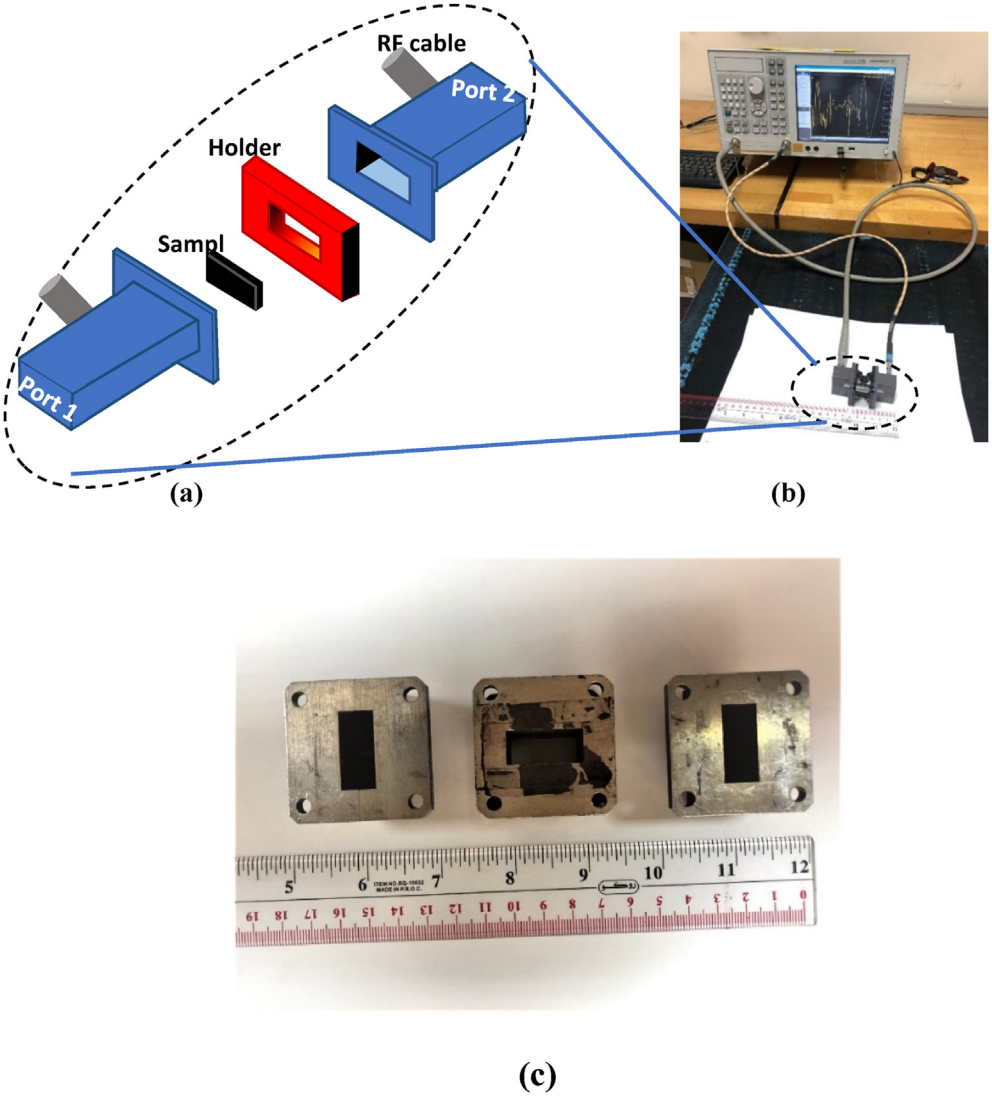

Fig. 9 – Setup for measurement of the microwave properties of samples: (a) detail of the waveguide structure when the three pieces are moved away from each other, (b) waveguide connected to the vector network analyzer using low-loss RF cables, and (c) disassembled waveguide structure.

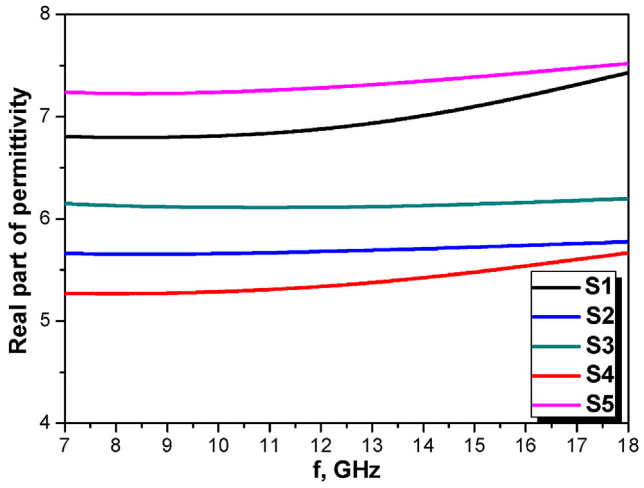

Fig. 10 – Values of the real part of the permittivity of S1–S5 H/S NCs over the 7–18 GHz range.

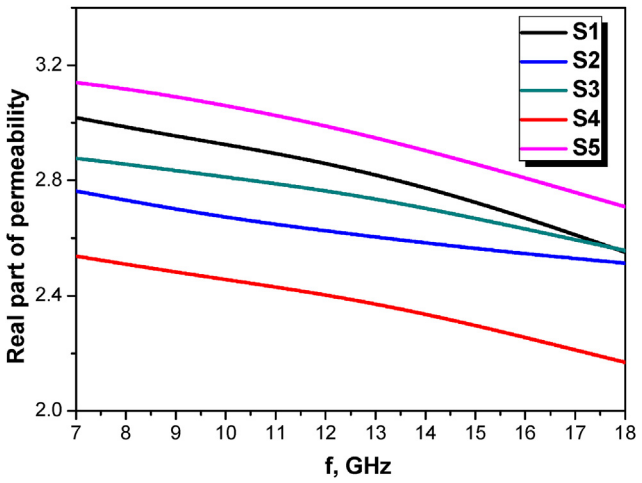

Fig. 12 – Values of the real part of the permeability of S1–S5 H/S NCs over the 7–18 GHz range.

case, the presence of a domain structure in the ferromagnet complicates the process, leading to the possibility of the appearance of several resonance peaks, and the resonant absorption of MW energy causes local heating. The ferromagnetic resonance frequency of a flat sample in a parallel external field is calculated using the Kittel equation:

$$f = \frac{\gamma}{2\pi}\sqrt{B(B+\mu_0 M)} \quad (1)$$

where M is the magnetization of the material.

The magnetization depends on the p_m vector of the magnetic moment for the entire set of atoms in a given volume of the material, V.

$$M = \frac{p_m}{V} \quad (2)$$

Accordingly, by increasing the number of ions in the material, the vector of the magnetic moment increases (with a constant volume), and the magnetization and frequency of absorption of the energy of the electromagnetic field increase.

The dipole moment can be calculated using following equation:

$$M_q = e \cdot r \quad (3)$$

where e is the charge of the partial dipole, and r is the distance between negative and positive charges.

Fig. 10 shows that an increase in the Ni content affects the permittivity of the mixture. For example, sample S5 has a nickel content of 0.8, which is the highest among all samples, while the copper and zinc contents are minimal at 0.1. Hence, S5 exhibits the highest dielectric constant. On the other hand, increasing the copper and zinc contents will lead to a rapid decrease in permittivity because the dipole moments for copper and zinc are opposite to the main dipole moment of nickel.

Owing to the differences in the shapes and polarizabilities of the f-, p-, and s-electronic orbitals, the center of the dipole moment is shifted towards nickel by r, which results in generation of the so-called homopolar moment of the dipole. An increase in nickel content accompanied by a decrease in the copper and zinc contents in the composite maximizes the real

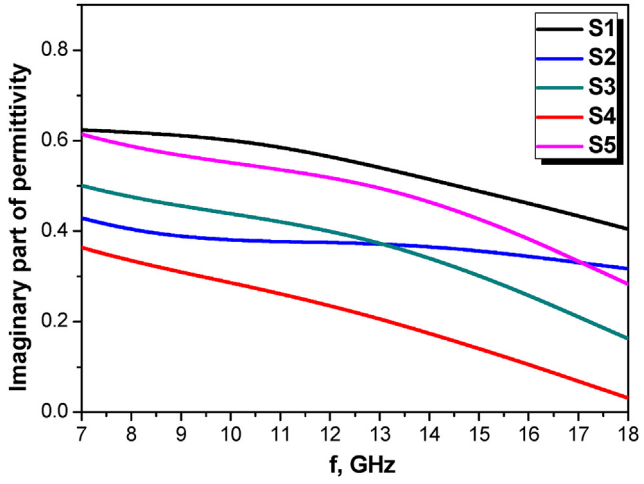

Fig. 11 – Values of the imaginary part of the permittivity of S1–S5 H/S NCs over the 7–18 GHz range.

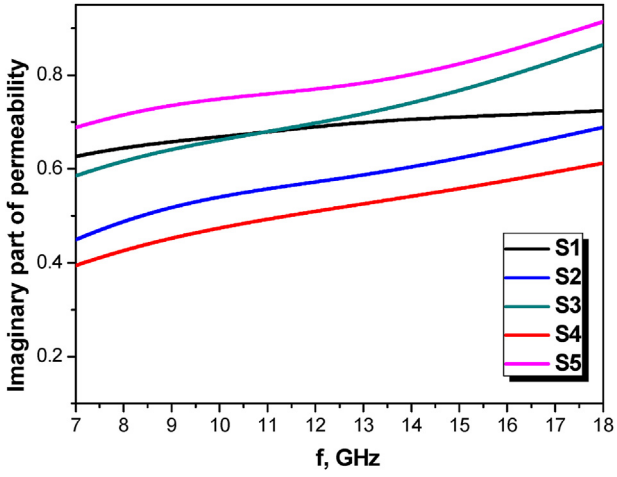

Fig. 13 – Values of the imaginary part of the permeability of the S1–S5 H/S NCs over the 7–18 GHz range.

part of the permittivity (ε′) over the entire frequency range (see Fig. 10).

The dielectric losses of materials are determined by the imaginary part of the permittivity (ε"). At lower frequencies, when dipole polarization exists, these losses are substantial. With increasing frequency, the orientations of the dipoles do not have time to change in the AC field. This results in transformation of the dipole polarization to a polarization due to the ion-relaxation processes. This type of polarization (i.e., ion relaxation) can be described by the ion shifts in the crystal lattice.

The permeability (μ) of the composites exhibits distinct peculiarities over the considered frequency range in a similar manner to the permittivity, as shown in Figs. 12 and 13. All of the studied samples behave like ferromagnets (where $\mu > 1$). Larmor's theorem can explain this change in permeability with frequency. Samples of a substance in a quiescent state exhibit a magnetic moment with a small value that does not drastically alter the whole magnitude of the permeability. On the other hand, when a time-varying magnetic field excites the substance, precession of the magnetic moment of electrons will begin according to Larmor's theorem.

Because nickel, copper, and zinc have practically the same number of electrons (they are located in series sequentially), an increase in the frequency provokes an increase in the precession of the electrons' magnetic moment. This results in an increase in the real part of the permeability (μ′). Because of the insignificant value of the magnetic moment of zinc, an increase in the Zn content marginally alters the global value of μ'. The number of electrons for the Ni ion is smaller than that for Cu. It is observed that an increase in the Cu concentration affects the total precession of the magnetic moments of the electrons insignificantly and increases the real part (μ′).

The increase in μ" with increasing x, y, and z contents can be clarified as follows: an increase in the frequency induces an increase in the precession of the magnetic moments of electrons and a growth in the energy expended to preserve the precessions, i.e., losses.

Herein, the reflection coefficient of a semi-infinite surface is calculated. Let the EM waves fall normally at the interface between two media: air and the material under study, whose parameters were measured as ε_2 and μ_2. In this case, the reflection coefficient is expressed as

$$R = \frac{\sqrt{\frac{\mu_2}{\varepsilon_2}} - 1}{\sqrt{\frac{\mu_2}{\varepsilon_2}} + 1} \tag{4}$$

To analyze the obtained values of the reflection coefficient, Fig. 14 shows the dependence of the reflection coefficient magnitude on the frequency, which can be expressed in decibels (dB) as

$$|R| = 20\ log\left(\frac{\sqrt{\frac{\mu_2}{\varepsilon_2}} - 1}{\sqrt{\frac{\mu_2}{\varepsilon_2}} + 1}\right) \tag{5}$$

where |R| is the reflectance magnitude, representing the ratio of the reflected voltage amplitude relative to the amplitude of the incident voltage in dB.

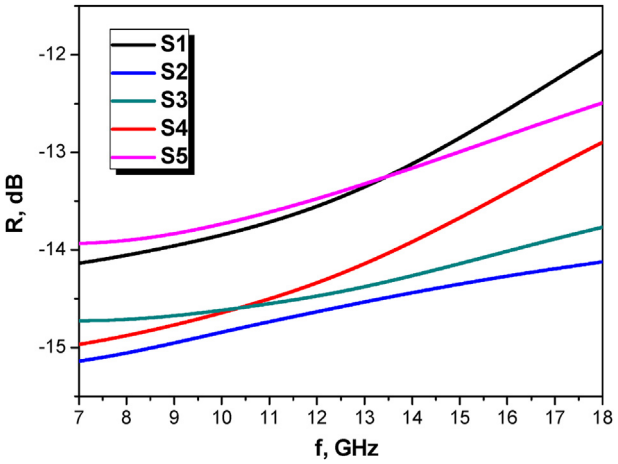

Fig. 14 – Frequency dispersions of the reflection losses of S1–S5 H/S NCs.

Fig. 14 shows the frequency dispersion of the reflection losses (R). It is evident that the value of the coefficient of the reflection is lower than −13 dB in the range of 7–14 GHz, which indicates that the produced nanocomposite materials can absorb adequate energy through losses in polarization. This behavior of small reflectivity suggests exciting applications in radar-based systems such as stealth aircraft with low observability in military applications.

4. Conclusion

A *one-pot* sol–gel auto-combustion approach was used to obtain S1–S5 $Sr_{0.5}Ba_{0.5}Eu_{0.01}Fe_{12}O_{19}/Ni_xCu_yZn_wFe_2O_4$ H/S NCs. The XRD results showed the formation of both hard and soft phases with crystal sizes in the range of 20 and 85 nm, respectively. The surface analysis showed aggregation of a hexagonal plate covered by a cluster of cubic particles, indicating the co-occurrence of hexaferrite and spinel ferrite. Analysis of the magnetic measurements revealed that the reversal in magnetization was not smooth, and the M–H curves did not present a single-phase character in the second quadrant. Furthermore, the plots of dM/dH versus H presented two separate peaks. Additionally, the calculated SQR values were lower than 0.5. All of these findings indicate that the exchange interaction between the two magnetic phases was incomplete. Maximum M_s values were obtained for the sample that contained the highest content of Zn and the same contents of Ni and Cu within the soft magnetic phase (i.e., H/S $Sr_{0.5}Ba_{0.5}Eu_{0.01}Fe_{11.99}O_{19}/Ni_{0.2}Cu_{0.2}Zn_{0.6}Fe_2O_4$). In contrast, H_c reached a maximum value for the sample that contained lower fractions of Zn and Cu and the highest fraction of Ni (i.e., H/S $Sr_{0.5}Ba_{0.5}Eu_{0.01}Fe_{11.99}O_{19}/Ni_{0.8}Cu_{0.1}Zn_{0.1}Fe_2O_4$). Investigations of the electrodynamic properties of the SrBaEu-hexaferrite/NiCuZn-spinel composites with fixed SrBaEu compositions and varying NiCuZn compositions were performed at frequencies of 7–18 GHz. The measurements were performed using the waveguide reflection/transmission method. S-parameters (S_{11}–S_{21}) were measured and used to

calculate the frequency dispersions of ε and μ (real and imaginary parts). It was observed that the stoichiometry of the NiCuZn ions in the spinel fraction critically influenced the electrodynamic properties. It was demonstrated that this type of composite effectively absorbed energy (>-13 dB) in the range of 7–14 GHz due to losses in polarization. This research opens a vast scope for applications in radar-absorbing technologies owing to the adequate level of absorption that must be close to the natural absorption of air media.

Declaration of Competing Interest

The authors declare that they have no known competing financial interests or personal relationships that could have appeared to influence the work reported in this paper.

Acknowledgments

This study was supported by the Deanship of Scientific Research of Imam Abdulrahman Bin Faisal University (Dammam, Saudi Arabia) through Grant No. 2020-164-IRMC. The authors also acknowledge support from the Center for Communication Systems and Sensing at KFUPM. Electromagnetic measurements and analysis were partially supported by the Russian Science Foundation (Agreement No. 21-79-10115).

REFERENCES

[1] Kozlovskiy AL, Kenzhina IE, Zdorovets MV. FeCo– Fe_2CoO_4/Co_3O_4 nanocomposites: phase transformations as a result of thermal annealing and practical application in catalysis. Ceram Int 2020;46(8):10262–9.
[2] Almessiere MA, Trukhanov AV, Slimani Y, You KY, Trukhanov SV, Trukhanova EL, et al. Correlation between composition and electrodynamics properties in nanocomposites based on hard/soft ferrimagnetics with strong exchange coupling. Nanomaterials 2019;9:202.
[3] Xia J, Wu X, Huang Y, Wu W, Liang J, Li Q. Enhancements of saturation magnetization and coercivity in $Ni_{0.5}Zn_{0.5}Fe_2O_4$/$SrFe_{12}O_{19}$ composite powders by exchange-coupling mechanism. J Mater Sci Mater Electron 2019;30:11682–93.
[4] Zdorovets MV, Kozlovskiy AL. Investigation of phase transformations and corrosion resistance in Co/CoCo2O4 nanowires and their potential use as a basis for lithium-ion batteries. Sci Rep 2019;9(1):16646.
[5] Meng XF, Hana QX, Sun YJ, Liu YF. Enhancements of saturation magnetization and coercivity in $Ni_{0.5}Zn_{0.5}Fe_2O_4$/$SrFe_{12}O_{19}$ composite powders by exchange-coupling mechanism. Ceram Int 2019;45:2504–8.
[6] Han QX, Meng XF, Lu CH. Exchange-coupled $Ni_{0.5}Zn_{0.5}Fe_2O_4$/$SrFe_{12}O_{19}$ composites with enhanced microwave absorption performance. J Alloys Compd 2018;768:742–9.
[7] Meng X, Han Q, Sun Y, Liu Y. Synthesis and microwave absorption properties of $Ni_{0.5}Zn_{0.5}Fe_2O_4$/$BaFe_{12}O_{19}$@ polyaniline composite. Ceram Int 2019;45:2504–8.
[8] Xia J, Ning Y, Luo Y, Chen W, Wu X, Wu W, et al. Structural and magnetic properties of soft/hard $NiFe_2O_4$@$SrCo_{0.2}Fe_{11.8}O_{19}$ core/shell composite prepared by the ball-milling-assisted ceramic process. J Mater Sci: Mater Electron 2018;29:13903–13.
[9] Afshar SS, Hasheminiasari M, Masoudpanah SM. Structural, magnetic and microwave absorption properties of $SrFe_{12}O_{19}$/$Ni_{0.6}Zn_{0.4}Fe_2O_4$ composites prepared by one-pot solution combustion method. J Magn Magn Mater 2018;466:1–6.
[10] Zhu Q, Jiang G, Riggs JM. Synthesis of magnetically exchange coupled $SrFe_{12}O_{19}$/FeCo core/shell particles through microwave-polyol process. Mater Lett 2016;163:270–3.
[11] Polley K, Alam T, Bera J. Synthesis and characterization of $BaFe_{12}O_{19}$-$CoFe_2O_4$ ferrite composite for high-frequency antenna application. J Aust Ceram Soc 2020;1:1–8.
[12] Szczygieł I, Winiarska K. Synthesis and characterization of manganese–zinc ferrite obtained by thermal decomposition from organic precursors. J Therm Anal Calorim 2014;115:471–7.
[13] Song F, Shen X, Liu M, Xiang J. One-dimensional $SrFe_{12}O_{19}$/$Ni_{0.5}Zn_{0.5}Fe_2O_4$ composite ferrite nanofibers and enhancement magnetic property. J Nanosci Nanotechnol 2011;11:6979–85.
[14] Petrecca M, Muzzi B, Oliveri SM, Albino M, Yaacoub N, Peddis D, et al. Optimizing the magnetic properties of hard and soft materials for producing exchange spring permanent magnets. J Phys D Appl Phys 2021;54:134003.
[15] Slimani Y, Algarou NA, Almessiere MA, Sadaqat A, Vakhitov MG, Klygach DS, et al. Fabrication of exchange coupled hard/soft magnetic nanocomposites: correlation between composition, magnetic, optical and microwave properties. Arab J Chem 2021;14:102992.
[16] Yu J, Bai L, Gao R. Effect of sintering temperature on magnetoelectric coupling in $0.2Ni_{0.9}Zn_{0.1}Fe_2O_4$-$0.8Ba_{0.9}Sr_{0.1}TiO_3$ composite ceramics. Process Appl Ceram 2020;14:336–45.
[17] Sugi S, Radhika S, Padma CM. Photocatalytic activity of pva mediated zinc-strontium ferrite composites. Wu Tan Hua Tan Ji Suan Ji Shu 2020;16:485–94.
[18] Xiong R, Li W, Fei C, Liu Y, Shi J. Exchange-spring behavior in $BaFe_{12}O_{19}$-$Ni_{0.5}Zn_{0.5}Fe_2O_4$ nanocomposites synthesized by a combustion method. Ceram Int 2016;42:11913–7.
[19] Kozlovskiy AL, Zdorovets MV. The study of the structural characteristics and catalytic activity of Co/CoCo2O4 nanowires. Comp B 2020;191:107968.
[20] Liu JP, Liu Y, Skomaski R, Sellmyer DJ. Magnetic hardening in SmCox–Co multilayers and nanocomposites. J Appl Phys 1999;85:4812–4.
[21] Goll D, Seeger M, Kronmuller H. Magnetic and microstructural properties of nano crystalline exchange coupled PrFeB permanent magnets. J Magn Magn Mater 1998;185:49–60.
[22] Jiang JS, Pearson JE, Liu ZY, Kabius B, Trasobares S, Miller DJ, et al. A new approach for improving exchange-spring magnets. J Appl Phys 2005;97:10 K311. 10K311-3.
[23] Davies JE, Hellwig O, Fullerton EE, Jiang JS, Bader SD, Zimanyi GT, et al. Anisotropy dependence of irreversible switching in Fe/ Sm Co and Fe Ni/ Fe Pt exchange spring magnet films. Appl Phys Lett 2005;86:262503.
[24] Feng W, Liu H, Hui P, Yang H, Li J, Wang JS. Preparation and properties of $SrFe_{12}O_{19}$/$ZnFe_2O_4$ core/shell nano-powder microwave absorber. Integrated Ferroelectrics Int J 2014;152:120–6.
[25] Li D, Wang F, Xia A. A facile way to realize exchange-coupling interaction in hard/soft magnetic composites. J Magn Magn Mater 2016;41:355–8.
[26] Hazra S, Ghosh N. Preparation of nano ferrites and their applications. J Nanosci Nanotechnol 2014;l14:1983–2000.
[27] Algarou NA, Slimani Y, Almessiere MA, Baykal A, Guner S, Manikandan A, et al. Enhancement on the exchange coupling behavior of $SrCo_{0.02}Zr_{0.02}Fe_{11.96}O_{19}$/$MFe_2O_4$ (M= Co,

Ni, Cu, Mn and Zn) as hard/soft magnetic nanocomposites. J Magn Magn Mater 2020;499:166308.
[28] Zdorovets MV, Kozlovskiy AL. Study of phase transformations in Co/$CoCo_2O_4$ nanowires. J Alloys Compd 2020;815:152450.
[29] Anantharamaiah PN, Rao BP, Shashanka HM, Chelvane JA, Khopkar V, Sahoo B. Role of Mg^{2+} and In^{3+} substitution on magnetic, magnetostrictive and dielectric properties of $NiFe_2O_4$ ceramics derived from nanopowders. Phys Chem Chem Phys 2021;23:1694–705.
[30] Zahid M, Siddique S, Anum R, Shakir MF, Nawab Y, Rehan ZA. M-Type barium hexaferrite-based nanocomposites for emi shielding application: a review. J Supercond Nov Magnetism 2021;5:1–27.
[31] Mehdipour M, Sholrollahi H. Comparison of microwave absorption properties of $SrFe_{12}O_{19}$, $SrFe_{12}O_{19}/NiFe_2O_4$ and $NiFe_2O_4$ particles. J Appl Phys 2013;113:043906.
[32] Hilczer A, Kowalska K, Markiewicz E, Adam P. Dielectric and magnetic response of $SrFe_{12}O_{19}$-$CoFe_2O_4$ composites obtained by solid state reaction. Mater Sci Eng B 2016;207:47–55.
[33] Ma Q, Ma Y, Zan F, Xu Y, Zheng G, Dai Z, et al. Complex exchange anisotropy behavior in Co_3O_4–$Ni_{0.6}Zn_{0.4}Fe_2O_4$ composite with different Co_3O_4 content. Mater Res Bull 2014;51:381–8.
[34] Varadan VK, Vinoy KJ, Gopalakrishnan S. Smart material systems and MEMS: design and development methodologies. John Wiley & Sons; 2006. p. 418.
[35] Golt MC. Magnetic and dielectric properties of magneto-dielectric materials consisting of oriented, iron flake filler within a thermoplastic host. University of Delaware; 2008.
[36] Yang Y, Liu L, Zhu H, Bao N, Ding J, Chen J, et al. Critical control of highly stable nonstoichiometric Mn–Zn ferrites with outstanding magnetic and electromagnetic performance for gigahertz high-frequency applications. ACS Appl Mater Interfaces 2020;12:16609–19.
[37] Luo Juhua, Xu Yang, Yao Wei, Jiang Cuifeng, Xu Jianguang. Synthesis and microwave absorption properties of reduced graphene oxide-magnetic porous nanospheres-polyaniline composites Comp. Sci Technol 2015;117:315–21.
[38] Luo Juhua, Lu Yue, Ji Hongru, Zhang Kang, Yu Ning. Investigation on the optimization, design and microwave absorption properties of BaTb0.2Eu0.2Fe11.6O19/PANI decorated on reduced graphene oxide nanocomposites. J Mater Sci 2019;54:6332–46.
[39] Hyde IV MW, Havrilla MJ. A nondestructive technique for determining complex permittivity and permeability of magnetic sheet materials using two flanged rectangular waveguides. Prog Electromagn Res. 2008;79:367–86.
[40] Zoughi R. Microwave non-destructive testing and evaluation principles. Germany: Springer Science & Business Media: Berlin/Heidelberg; 2012. 978-94-015-1303-6.
[41] Hasar UC. Nondestructive testing of hardened cement specimens at microwave frequencies using a simple free-space method. NDT E Int 2009;42:550–7.
[42] Yousefi L, Attia H, Ramahi O. Broadband experimental characterization of artificial magnetic materials based on a microstrip line method. Prog Electromagn Res. 2009;90:1–13.
[43] Kharkovsky S, Zoughi R. Microwave and millimeter wave nondestructive testing and evaluation—overview and recent advances. IEEE Instrum Meas Mag 2007;10:26–38.
[44] Zhang H, Gao B, Tian GY, Woo WL, Bai L. Metal defects sizing and detection under thick coating using microwave NDT. NDT E Int 2013;60:52–61.
[45] Chen L-F, Ong CK, Neo CP, Varadan VV, Varadan VK. Microwave electronics: measurement and materials characterization, vol. 30. Hoboken, NJ, USA: John Wiley & Sons; 2004.
[46] Liu C, Kan X, Liu X, Feng S, Hu J, Wang W, et al. Influence of the Eu substitution on the structure and magnetic properties of the Sr-hexaferrites. Ceram Int 2020;46:171–9.
[47] Zafar A, ur Rahman A, Shahzada S, Anwar S, Khan M, Nisar A, et al. Electrical and magnetic properties of nano-sized Eu doped barium hexaferrites. J Alloys Compd 2017;727:683–90.
[48] Thangjam B, Soibam I. Comparative study of structural, Electrical,and magnetic behaviour of Ni-Cu-Zn nanoferrites sintered by microwave and conventional techniques. J Nanomater 2017:1–10.
[49] Venkatesh D, Vara Prasad BBVS, Ramesh KV, Ramesh MNV. Magnetic properties of Cu^{2+} substituted Ni–Zn nano-crystalline ferrites synthesized in citrate-gel route. J Inorg Organomet Polym Mater 2020;30:2057–66.
[50] Von Hippel AR. Dielectric materials and applications, vol. 2. Dedham, MA, USA: Artech House; 1954.
[51] Torkian S, Ghasemi A, Razavi RS. Magnetic properties of hard-soft $SrFe_{10}Al_2O_{19}/Co_{0.8}Ni_{0.2}Fe_2O_4$ ferrite synthesized by one-pot sol–gel auto-combustion. J Magn Magn Mater 2016;416:408–16.
[52] Fan D, Chen LQ. Topological evolution during coupled grain growth and Ostwald ripening in volume-conserved 2-D two-phase polycrystals. Acta Mater 1997;45:4145.
[53] Hsu WC, Chen SC, Kuo PC, Lie CT, Tsai WS. Preparation of NiCuZn ferrite nanoparticles from chemical co-precipitation method and the magnetic properties after sintering. Mater Sci Eng B Solid-State Mater Adv Technol 2004;111:142–9.
[54] Sujatha C, Venugopal Reddy K, Sowri Babu K, Ramachandra Reddy A, Rao KH. Effect of sintering temperature on electromagnetic properties of NiCuZn ferrite. Ceram Int 2013;39:3077–86.
[55] Karisma AD, Shinokawa Y, Fukasawa T, Ishigami T, Fukui K. Synthesis of NiCuZn ferrite nanoparticles from metallic nitrate solutions using the microwave direct denitration method and evaluation of its properties, Part. Sci Technol 2020:1–9.
[56] Yu L, Cao S, Liu Y, Wang J, Jing C, Zhang J. Thermal and structural analysis on the nanocrystalline NiCuZn ferrite synthesis in different atmospheres. J Magn Magn Mater 2006;301:100–6.
[57] Slimani Y, Unal B, Almessiere MA, Korkmaz AD, Shirsath SE, Yasin G, et al. Investigation of structural and physical properties of Eu^{3+} ions substituted $Ni_{0.4}Cu_{0.2}Zn_{0.4}Fe_2O_4$ spinel ferrite nanoparticles prepared via sonochemical approach. Results Phys 2020;17:103061.
[58] Jacobo SE, Aphesteguy JC, Shegoleva NN, Kurlyandskaya GV. Structural and magnetic properties of nanoparticles of NiCuZn ferrite prepared by the self-combustion method. In: Solid state phenom. Trans Tech Publications Ltd; 2011. p. 333–40.
[59] Slimani Y, Almessiere MAA, Korkmaz ADD, Guner S, Güngüneş H, Sertkol M, et al. $Ni_{0.4}Cu_{0.2}Zn_{0.4}TbxFe_{2-x}O_4$ nanospinel ferrites: ultrasonic synthesis and physical properties, Ultrason. Sonochem 2019;59:104757.
[60] Slimani Y, Almessiere MA, Sertkol M, Shirsath SE, Baykal A, Nawaz M, et al. Structural, magnetic, optical properties and cation distribution of nanosized Ni0.3Cu0.3Zn0.4TmxFe2−xO4 ($0.0 \leq x \leq 0.10$) spinel ferrites synthesized by ultrasound irradiation. Ultrason Sonochem 2019;57:203–11.
[61] Almessiere MA, Slimani Y, Trukhanov AV, Demir Korkmaz A, Guner S, Akhtar S, et al. Effect of Nd-Y co-substitution on structural, magnetic, optical and microwave properties of NiCuZn nanospinel ferrites. J Mater Res Technol 2020;9:11278–90.

[62] Almessiere MA, Slimani Y, Demir Korkmaz A, Baykal A, Albetran H, Saleh TA, et al. A study on the spectral, microstructural, and magnetic properties of Eu–Nd double-substituted Ba0.5Sr0.5Fe12O19 hexaferrites synthesized by an ultrasonic-assisted approach. Ultrason Sonochem 2020;62:104847.
[63] Slimani Y, Almessiere MA, Guner S, Alahmari FS, Yasin G, Trukhanov AV, et al. Influence of Tm–Tb substitution on magnetic and optical properties of Ba–Sr hexaferrites prepared by ultrasonic assisted citrate sol-gel approach. Mater Chem Phys 2020;253:123324.
[64] Slimani Y, Almessiere MA, Güner S, Kurtan U, Baykal A. Impacts of sol-gel auto-combustion and ultrasonication approaches on structural, magnetic, and optical properties of Sm-Tm Co-substituted Sr0.5Ba0.5Fe12O19 nanohexaferrites: comparative study. Nanomaterials 2020;10:272.
[65] Khademi F, Poorbafrani A, Kameli P, Salamati H. Structural, magnetic and microwave properties of Eu-doped barium hexaferrite powders. J Supercond Nov Magnetism 2012;25:525–31.
[66] Ali I, Islam MU, Awan MS, Ahmad M, Iqbal MA. Structural and magnetic properties of nano-structured Eu^{3+} substituted M-Type hexaferrites synthesized by sol-gel auto-combustion technique. J Supercond Nov Magnetism 2013;26:3315–23.
[67] Neupane D, Ghimire M, Adhikari H, Lisfi A, Mishra SR. Synthesis and magnetic study of magnetically hard-soft SrFe12-yAlyO19 - x Wt.% Ni0.5Zn0.5Fe2O4 nanocomposites. AIP Adv 2017;7:055602.
[68] Shan ZS, Liu JP, Chakka VM, Zeng H, Jiang JS. Energy barrier and magnetic properties of exchange-coupled hard-soft bilayer. IEEE Trans Magn 2002:2907–9.
[69] Skomski R, Coey JMD. Exchange coupling and energy product in random two-phase Aligned magnets. IEEE Trans Magn 1994;30:607–9.
[70] Almessiere MA, Slimani Y, Baykal A. Exchange spring magnetic behavior of Sr0.3Ba0.4Pb0.3Fe12O19/(CuFe2O4)x nanocomposites fabricated by a one-pot citrate sol-gel combustion method. J Alloys Compd 2018;762:389–97.
[71] Song F, Shen X, Liu M, Xiang J. Microstructure, magnetic properties and exchangecoupling interactions for one-dimensional hard/soft ferrite nanofibers. J Solid State Chem 2012;185:31–6.
[72] Sun Y, Gao R, Han B, Liu M, Han G, Feng W. Exchange-coupling interaction, effective anisotropy and magnetic property of nano-magnetic materials. Prog Nat Sci 2007;17:131–7.
[73] Algarou NA, Slimani Y, Almessiere MA, Rehman S, Younas M, Unal B, et al. Developing the magnetic, dielectric and anticandidal characteristics of $SrFe_{12}O_{19}/(Mg_{0.5}Cd_{0.5}Dy_{0.03}Fe_{1.97}O_4)_x$ hard/soft ferrite nanocomposites. J Taiwan Inst Chem Eng 2020;113:344–62.
[74] Mathews SA, Babu DR, Saravanan P, Hayakawa Y. Microwave absorption studies of (Ba0.5Sr0.5Fe12O19)1-x/(NiFe2O4)x hard/soft ferrite nanocomposites. Mater Chem Phys 2020;252:123063.
[75] Algarou NA, Slimani Y, Almessiere M, Baykal A. Exchange-coupling behavior in SrTb0.01Tm0.01Fe11.98O19/(CoFe2O4)x hard/soft nanocomposites. New J Chem 2020;44:5800–8.
[76] Almessiere MA, Slimani Y, Baykal A. Structural, morphological and magnetic properties of hard/soft SrFe12-xVxO19/(Ni0.5Mn0.5Fe2O4)y nanocomposites: effect of vanadium substitution. J Alloys Compd 2018;767:966–75.
[77] Algarou NA, Slimani Y, Almessiere MA, Alahmari FS, Vakhitov MG, Klygach DS, et al. Magnetic and microwave properties of SrFe12O19/MCe0.04Fe1.96O4 (M = Cu, Ni, Mn, Co and Zn) hard/soft nanocomposites. J Mater Res Technol 2020;9:5858–70.
[78] Algarou NA, Slimani Y, Almessiere MA, Sadaqat A, Trukhanov AV, Gondal MA, et al. Functional Sr0.5Ba0.5Sm0.02Fe11.98O4/x(Ni0.8Zn0.2Fe2O4) hard–soft ferrite nanocomposites: structure, magnetic and microwave properties. Nanomaterials 2020;10:2134.
[79] Algarou NA, Slimani Y, Almessiere MA, Güner S, Baykal A, Ercan I, et al. Exchange-coupling effect in hard/soft SrTb0.01Tm0.01Fe11.98O19/AFe2O4 (where A = Co, Ni, Zn, Cu and Mn) composites. Ceram Int 2020;46:7089–98.
[80] Nicolson AM, Ross GF. Measurement of the intrinsic properties of materials by time-domain techniques. IEEE Trans Instrum Meas 1970;19:377–82.
[81] Afsar MN, Birch JR, Clarke RN, Chantry GW. The measurement of the properties of materials. Proc IEEE 1986;74:183–99.
[82] Costa F, Borgese M, Degiorgi M, Monorchio A. Electromagnetic characterization of materials by using transmission/reflection (T/R) devices. Electronics 2017;6:95.